

EDGE ARTICLE

Cite this: *Chem. Sci.*, 2020, 11, 1290

All publication charges for this article have been paid for by the Royal Society of Chemistry

Received 4th October 2019
Accepted 12th December 2019

DOI: 10.1039/c9sc04992d

rsc.li/chemical-science

Manipulating nonadiabatic conical intersection dynamics by optical cavities†

Bing Gu *^a and Shaul Mukamel *^b

Optical cavities hold great promise to manipulate and control the photochemistry of molecules. We demonstrate how molecular photochemical processes can be manipulated by strong light–matter coupling. For a molecule with an inherent conical intersection, optical cavities can induce significant changes in the nonadiabatic dynamics by either splitting the pristine conical intersections into two novel polaritonic conical intersections or by creating light-induced avoided crossings in the polaritonic surfaces. This is demonstrated by exact real-time quantum dynamics simulations of a three-state two-mode model of pyrazine strongly coupled to a single cavity photon mode. We further explore the effects of external environments through dissipative polaritonic dynamics computed using the hierarchical equation of motion method. We find that cavity-controlled photochemistry can be immune to external environments. We also demonstrate that the polariton-induced changes in the dynamics can be monitored by transient absorption spectroscopy.

1 Introduction

Photochemical processes are routinely manipulated by chemical modification and external laser driving. Recently, optical cavities have emerged as a new means to manipulate and control these processes.^{1,2} Vacuum fluctuations in nanoscale fabricated cavities can influence molecular potential energy surfaces even without external fields. Substantial couplings can be induced between electronic or vibrational transitions in the molecule and the photon mode confined in the optical cavity. The strong coupling regime is realized when the light–matter coupling is stronger than the loss rate of the cavity mode and the decoherence rate of the molecule. In this regime, the molecular degrees of freedom mix with the cavity photon forming hybrid light–matter states known as polaritons carrying both characters of matter and light. Recent experiments have realized this regime even when the field is in the vacuum state^{3–7} for a single molecule,⁸ and it has been experimentally demonstrated that the strong coupling can alter the branching ratio of two competing reaction pathways in a molecule,⁹ induce long-range energy transfer,^{4,5} enhance Raman scattering,¹⁰ and modify a chemical reaction rate. These experiments have triggered extensive theoretical investigations,^{11–27} which suggested an even

wider variety of chemical processes that can potentially be manipulated by optical cavities including photochemistry.^{1,2}

Cavity photochemistry happens in a very different way under strong coupling. Without the cavity, the nonadiabatic molecular dynamics after photoexcitation is dictated by the Born–Oppenheimer adiabatic potential energy surfaces (APES). For many photochemical reactions, the APESs contain conical intersections (CI), which offer a funnel for the nuclear wavepacket to relax nonradiatively to lower electronic states. In the strong coupling regime, the photoreactions are determined by the polaritonic potential energy surfaces (PPES). These are defined similarly to the APES but with the polaritonic states playing the role of adiabatic states. As demonstrated in recent theoretical studies,^{1,2,12,28} the PPESs can look very different from the APESs and may contain more complex features, in particular when many molecules interact with the same cavity mode.²⁹

While previous efforts had focused on light-induced conical intersections in optical cavities,^{1,29,30} studies on how strong light–matter interaction influence the nonadiabatic dynamics of molecules with inherent CIs are scarce.³¹ Here we investigate how optical cavities can alter the nonadiabatic dynamics through a conical intersection, how external dissipative environments affect the photodynamics, and how polaritonic dynamics can be probed by nonlinear spectroscopy. We first simulate the exact real-time quantum dynamics of a three-state two-mode model of pyrazine interacting with a single cavity photon mode with a complete basis set in the polaritonic space. We then simulate the dissipative dynamics of this polaritonic system coupled to an external environment using the hierarchical equation of motion approach.^{32,33} Finally we compute the transient absorption spectrum of this polaritonic system.

^aDepartment of Chemistry, University of California, Irvine, CA 92697, USA. E-mail: bingg@uci.edu

^bDepartment of Chemistry, Physics and Astronomy, University of California, Irvine, CA 92697, USA. E-mail: smukamel@uci.edu

† Electronic supplementary information (ESI) available: (i) Theory and computational protocol of transient absorption spectroscopy for polaritonic chemistry, and (ii) the hierarchical equations of motion method, and relation between spectral density and environment correlation function [eqn (13)]. See DOI: 10.1039/c9sc04992d



The pyrazine model contains three electronic states $\{|\psi_k\rangle, k = 0, 1, 2\}$ and a conical interaction (CI) exist between $|\psi_1\rangle$ and $|\psi_2\rangle$ that leads to ultrafast non-radiative relaxation of electronic excitation. When tuned to the $|\psi_0\rangle \leftrightarrow |\psi_1\rangle$ transition (case I), the optical cavities can split the pristine CI in the APESs into two novel polaritonic CIs in the PPESs. This leads to significant changes of the nonadiabatic dynamics, including creating a channel for direct electronic relaxation to the ground state that can only occur by radiative emission in pristine molecules. In turn, when the cavity photon couples to the $|\psi_1\rangle \leftrightarrow |\psi_2\rangle$ transition (case II), it can create avoided crossings in the PPESs while leaving the pristine CI intact. This cavity-induced crossing provides an additional relaxation channel leading to faster relaxation dynamics.

To monitor the nonadiabatic dynamics of the nuclear wavepacket moving through the CI, we use transient absorption spectroscopy (TAS). This pump-probe technique can reveal the level-populations in the course of non-adiabatic molecular dynamics. Our simulations demonstrate that the cavity-induced changes in the non-adiabatic dynamics can be observed by TAS.

We further explore the effects of external environments on the cavity control. It is found that the environment can have a deleterious effects on the polaritonic dynamics in case I, while in case II, the cavity control is immune to environmental effects. This different behavior of the environments can be attributed to the decoherence timescale.

2 Theory and computational protocol

2.1 Hamiltonian

The Hamiltonian of a molecule placed in an optical cavity, consists of the molecular Hamiltonian H_M , the cavity photon Hamiltonian H_C , and the cavity-matter interaction H_{CM} , and the classical light-matter interaction $H_{LM}(t)$

$$H = H_M + H_C + H_{CM} + H_{LM}(t). \quad (1)$$

The linear-vibronic coupling model of pyrazine developed in ref. 34 includes three electronic states and two vibrational modes that strongly couple to the electronic motion. It has been widely used to study the nonadiabatic dynamics of pyrazine through the CI.^{35,36} In the diabatic representation, the molecular Hamiltonian reads

$$H_M = h_0|\psi_0\rangle\langle\psi_0| + \sum_{k=1,2} h_k|\psi_k\rangle\langle\psi_k| + \lambda Q_c(|\psi_1\rangle\langle\psi_2| + \text{H.c.}) \quad (2)$$

with $h_k = h_0 + E_k + \kappa_k Q_t$, $h_0 = \sum_{\sigma=t,c} \hbar\Omega_\sigma(a_\sigma^\dagger a_\sigma + 1/2)$ and H.c.

stands for the Hermitian conjugate. Here Ω_σ and Q_σ denote, respectively, the frequency and dimensionless coordinate of the σ -

th vibrational mode ($\sigma = c$ for the coupling mode and $\sigma = t$ for the tuning mode), $\{|\psi_k\rangle\}$ are the diabatic electronic states, E_k is the vertical excitation energy at the Frank-Condon point for k -th electronic state, κ_k are the intra-state electron-vibrational coupling constant, and λ denotes the interstate coupling strength. The parameters in H_M are³⁵ $\hbar\omega_c = 118$ meV, $\hbar\omega_t = 74$ meV, $E_1 = 3.94$ eV, $E_2 = 4.84$ eV, $\kappa_1 = -105$ meV, $\kappa_2 = 149$ meV.

The cavity Hamiltonian is given by

$$H_C = \hbar\omega_{\text{cav}} \left(a_{\text{cav}}^\dagger a_{\text{cav}} + \frac{1}{2} \right) \quad (3)$$

where ω_{cav} is the resonance frequency of the single cavity mode and a_{cav} (a_{cav}^\dagger) is the annihilation (creation) operator of the cavity photon. The cavity-molecule interaction is described by the electric-dipole coupling

$$H_{CM} = \sum_{i<j} g_{ij}(\mathbf{R}) (a_{\text{cav}}^\dagger + a_{\text{cav}}) (|\psi_j\rangle\langle\psi_i| + \text{H.c.}) \quad (4)$$

where g is the coupling strength and \mathbf{R} denotes nuclear coordinates. Invoking the rotating-wave approximation (RWA) and the Condon approximation for the transition dipole in the diabatic representation (*i.e.*, neglecting the nuclear dependence of the transition dipole moment among diabatic states), the cavity-molecule interaction becomes

$$H_{CM} = \sum_{i<j} g_{ij} (a_{\text{cav}} |\psi_j\rangle\langle\psi_i| + \text{H.c.}). \quad (5)$$

The classical light-matter interaction $H_{LM}(t)$ contains the interaction between the molecule and light pulses used in the TAS optical measurement – an actinic and a probe pulse (see the ESI†).

2.2 Nonadiabatic polariton dynamics

The nonadiabatic dynamics of pyrazine in the optical cavities is simulated numerically exactly by solving the time-dependent Schrödinger equation in a complete basis set of the full polaritonic space – the direct product of the electronic space, vibrational space for the coupling and tuning modes, and the cavity photon space. More precisely, a polaritonic basis function is constructed as a direct product of the diabatic electronic state $|\psi_k\rangle$, number state of the cavity photon mode $|n_{\text{cav}}\rangle$, the number state of the coupling vibrational mode $|n_c\rangle$ and the number state of the tuning vibrational mode $|n_t\rangle$, *i.e.*,

$$|kn_{\text{cav}}n_cn_t\rangle = |\psi_k\rangle \otimes |n_{\text{cav}}\rangle \otimes |n_c\rangle \otimes |n_t\rangle \quad (6)$$

In this basis set, the matrix elements of H in the absence of classical laser pulses is given by

$$\begin{aligned} H_{kn_{\text{cav}}n_cn_t, k'n_{\text{cav}}n'_cn'_t} &= \delta_{kk'} \delta_{n_{\text{cav}}n'_{\text{cav}}} \delta_{n_cn'_c} \delta_{n_t n'_t} (E_k + \hbar\omega_{\text{cav}}(n_{\text{cav}} + 1/2) + \hbar\Omega_c(n_c + 1/2) + \hbar\Omega_t(n_t + 1/2)) \\ &+ \delta_{kk'} \delta_{n_{\text{cav}}n'_{\text{cav}}} \delta_{n_cn'_c} K_k X_{n_t n'_t} + (\delta_{k,k'-1} + \delta_{k,k'+1}) \delta_{n_{\text{cav}}n'_{\text{cav}}} \delta_{n_t n'_t} \lambda X_{n_c n'_c} \\ &+ g_{kk'} \left(\delta_{k,k'+1} \sqrt{n_{\text{cav}}} \delta_{n_{\text{cav}}n'_{\text{cav}}-1} + \delta_{k,k'-1} \sqrt{n_{\text{cav}}} \delta_{n_{\text{cav}}n'_{\text{cav}}+1} \right) \delta_{n_cn'_c} \delta_{n_t n'_t}, \end{aligned} \quad (7)$$

Here X is the position matrix elements in the number state basis

$$X_{nn'} = \delta_{n,n'+1} \sqrt{\frac{n}{2}} + \delta_{n,n'-1} \sqrt{\frac{n'}{2}}$$

2.3 The polaritonic potential energy surfaces

Multiple theoretical frameworks have been developed for the dynamics in optical cavities.^{1,37} The nonadiabatic polaritonic dynamics presented here is most conveniently understood in the PPEs. The PPEs are analogous to the APESs with the polaritonic states replacing the adiabatic electronic states. Under the separation of timescales of the electron-photon and the nuclear motion (Born–Oppenheimer-like approximation), the polaritonic states are defined as the eigenstates of the polaritonic Hamiltonian $H_p(\mathbf{r}, \mathbf{q}; \mathbf{R}) = H_{el}(\mathbf{r}; \mathbf{R}) + H_C(\mathbf{q}) + H_{CM}(\mathbf{r}, \mathbf{q}; \mathbf{R})$ which depends parametrically on the nuclear configuration

$$H_p(\mathbf{r}, \mathbf{q}; \mathbf{R}) |\Phi_n(\mathbf{R})\rangle = E_n(\mathbf{R}) |\Phi_n(\mathbf{R})\rangle \quad (8)$$

where \mathbf{r} , \mathbf{q} , \mathbf{R} denotes the electronic, photonic, and nuclear coordinates, respectively. Here $H_{el} = H_M - T_n$ is the electronic (or Born–Oppenheimer) Hamiltonian consisting of the electronic kinetic energy operator, electron–electron interaction, electron–nucleus interaction, and nuclei–nuclei interaction, *i.e.*, full molecular Hamiltonian without the nuclear kinetic energy. The polaritonic states reside in the composite space of the electronic and photonic subspaces, and can be expanded in the product basis set of the electronic states and photon Fock states, *i.e.*, $|\Phi_\lambda(\mathbf{R})\rangle = \sum_{k,n} C_{\lambda, kn}(\mathbf{R}) |\psi_k\rangle \otimes |n\rangle$, where the expansion coefficients can be obtained by solving eqn (8).

Alternatively, one can define a potential energy surface in the joint photon–nuclear space

$$H_p(\mathbf{r}; \mathbf{q}, \mathbf{R}) |\Phi_n(\mathbf{q}, \mathbf{R})\rangle = E_n(\mathbf{q}, \mathbf{R}) |\Phi_n(\mathbf{q}, \mathbf{R})\rangle \quad (9)$$

This can be useful for numerical simulations of polaritonic dynamics,³⁸ especially in the ultrastrong coupling regime where rotating wave approximation does not apply.

2.4 Effects of the external environment

Polaritonic systems inevitably interact with external environments, which can induce significant changes in their dynamics through energy relaxation and decoherence. The environment for the cavity photon are the photonic modes outside the cavity accessible *via* the imperfect reflections of the cavity mirrors. This interaction leads to a finite lifetime of the cavity photon mode. For femtosecond dynamics we can neglect the slower decay of the cavity mode. However, the environment for the molecular motion (*e.g.*, solvent) may have a large influence on the nonadiabatic polaritonic dynamics through ultrafast electronic decoherence processes.^{39–41}

We introduce an external environment $H_B = \sum_{\alpha} \hbar \omega_{\alpha} \left(a_{\alpha}^{\dagger} a_{\alpha} + \frac{1}{2} \right)$ consisting of a collection of harmonic oscillators with frequencies $\{\omega_{\alpha}\}$ described by the creation a_{α}^{\dagger} and annihilation operators a_{α} . The molecule–bath coupling

describing the decoherence effects between two electronic states $|\psi_i\rangle$ and $|\psi_j\rangle$ is given by

$$H_{MB} = S \otimes B = \sum_{\alpha} g_{\alpha} (|\psi_j\rangle \langle \psi_j| - |\psi_i\rangle \langle \psi_i|) (a_{\alpha}^{\dagger} + a_{\alpha}) \quad (10)$$

where we have introduced the system and bath operator $S = |\psi_j\rangle \langle \psi_j| - |\psi_i\rangle \langle \psi_i|$ and $B = \sum_{\alpha} g_{\alpha} (a_{\alpha}^{\dagger} + a_{\alpha})$. The influence of the environment on the molecule is encoded in the spectral density $J(\omega) \equiv \pi \sum_{\alpha} |g_{\alpha}|^2 \delta(\omega - \omega_{\alpha})$. We assume an Ohmic spectral density with a Lorentz–Drude cutoff

$$J(\omega) = 2\lambda\omega\gamma/(\omega^2 + \gamma^2) \quad (11)$$

where γ is the cutoff frequency and λ is the reorganization energy characterizing the system–bath coupling strength.

To account for the non-Markovian effects of the environment, we use the non-perturbative hierarchical equation of motion method.⁴² In this method, the reduced dynamics of the primary polaritonic system is described by a set of coupled differential equations ($\hbar = 1$; see the ESI† for a summary of this technique)

$$\dot{\rho}_n(t) = (-i\mathcal{L}_0 - n\gamma)\rho_n(t) - i\mathcal{S}^{-}\rho_{n-1}(t) - in\mathcal{V}\rho_{n+1}(t), \quad (12)$$

where $\mathcal{S}^{\pm}A = [S, A]_{\pm} = SA \pm AS$, $\mathcal{L}_0A = [H_0, A]$, $\mathcal{V} = \text{Re}[C(0)]\mathcal{S}^{-} + i\text{Im}[C(0)]\mathcal{S}^{+}$ are superoperators defined in the Liouville space, and $\{\rho_n, n = 0, 1, \dots\}$ are the auxiliary density operators with the first element corresponding to the reduced density matrix of the system $\rho_S(t) = \rho_0(t)$. Here $C(t) = \langle B_1(t)B \rangle$ is the environment time-correlation function where $B_1(t) = e^{+iH_B t} B e^{-iH_B t}$ is the bath operator B in the interaction picture of H_B . For environments at thermal equilibrium with inverse temperature $\beta = 1/(k_B T)$, it can be evaluated from the spectral density (details can be found in the ESI†)

$$C(t) = \frac{1}{\pi} \int_0^{\infty} (\coth(\beta\hbar\omega/2)\cos(\omega t) - i\sin(\omega t))J(\omega)d\omega \quad (13)$$

In the high-temperature limit $\beta\hbar\gamma < 1$, $\coth(\beta\hbar\omega/2) \approx 2/(\beta\hbar\omega)$ and the correlation function becomes

$$C(t) = \left(\frac{2\lambda}{\beta\hbar} - i\lambda\gamma \right) e^{-\gamma t} \quad (14)$$

2.5 The transient absorption signal

The polaritonic nonadiabatic dynamics typically occurs in the femtosecond timescale. Therefore, ultrafast time-resolved spectroscopy such as TAS can unveil the dynamic features induced by the strong light–matter coupling in optical cavities. TAS is a pump–probe technique capable of providing useful information on the population changes of excited molecules.⁴³ The molecule is first excited to an electronically excited state by an ultrashort pump pulse, and after a certain delay time T , a probe pulse interrogates the molecule by measuring the state-occupation changes. The theory for TAS for molecules in cavities and the computational details are given in the ESI.†

3 Results and discussion

3.1 Polaritonic dynamics

Because the pyrazine model contains three electronic states, there are several ways the molecule can be coupled to the cavity. In the following we consider two scenarios that lead to distinct polaritonic nonadiabatic dynamics.

We first assume that the cavity photon mode couples to the $|\psi_0\rangle \leftrightarrow |\psi_1\rangle$ transition. The cavity resonant frequency $\omega_{\text{cav}} = 4.3$ eV is close to the transition energy $|\psi_0\rangle \rightarrow |\psi_{1/2}\rangle$ at the CI point. The polaritonic surfaces are shown in Fig. 1c for the cavity–molecule coupling strength $g_{01} = 124$ meV. The electronic state population dynamics at different cavity–molecule coupling strength is shown in Fig. 2. The molecule is prepared at electronic state $|\psi_2\rangle$. The population dynamics of states $|\psi_1\rangle$ and $|\psi_0\rangle$ are shown in Fig. 2a and b, respectively, and the average value of the tuning mode is shown in Fig. 2c. Without the cavity, the nuclear wavepacket traverses through the CI and, due to the strong electron–nuclear coupling, the electronic excitation relaxes to $|\psi_1\rangle$ within 30 fs, see also Fig. 1b for the APESs of the model pyrazine without cavity–molecule coupling. The ground electronic state $|\psi_0\rangle$ is not populated during the dynamics as it is decoupled from the two excited electronic states.

When the cavity photon mode is coupled to the molecular transition $|\psi_0\rangle \leftrightarrow |\psi_1\rangle$, the electronic excitation directly relaxes back to the ground state as shown in Fig. 2b, in contrast to the nonadiabatic dynamics of the bare molecule. This implies that the strong light–matter coupling creates a channel for such relaxation process. The relaxation to the ground state is accompanied by the decrease of populations in the first electronic state with the overall

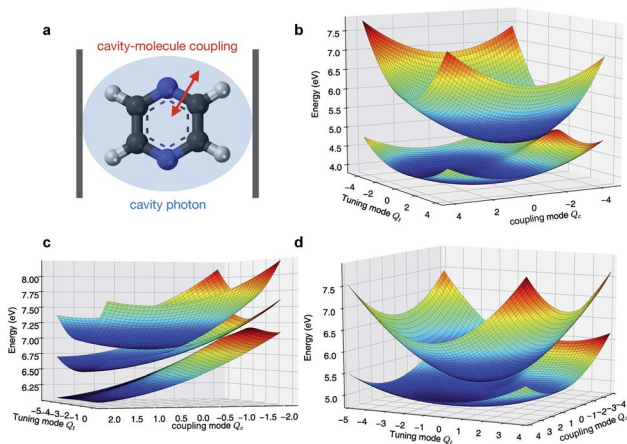


Fig. 1 Born–Oppenheimer (adiabatic) and polaritonic potential energy surfaces of the pyrazine model coupled to the cavity photon mode. The adiabatic and polaritonic surfaces are computed by diagonalizing the electronic and polaritonic Hamiltonian, respectively, scanning the nuclear configurations. (a) Schematic of the pyrazine molecule placed inside an optical cavity. (b) Adiabatic potential energy surfaces of the first and second excited states. (c) Polaritonic surfaces (relevant to the dynamics) when the cavity mode couples to the $|\psi_0\rangle \leftrightarrow |\psi_1\rangle$ transition. Here $\omega_{\text{cav}} = 4.3$ eV and $g_{01} = 124$ meV. (d) Same as (c) but for the cavity photon mode coupling to the $|\psi_1\rangle \leftrightarrow |\psi_2\rangle$ transition. Here $\omega_{\text{cav}} = 0.62$ eV and $g_{12} = 124$ meV.

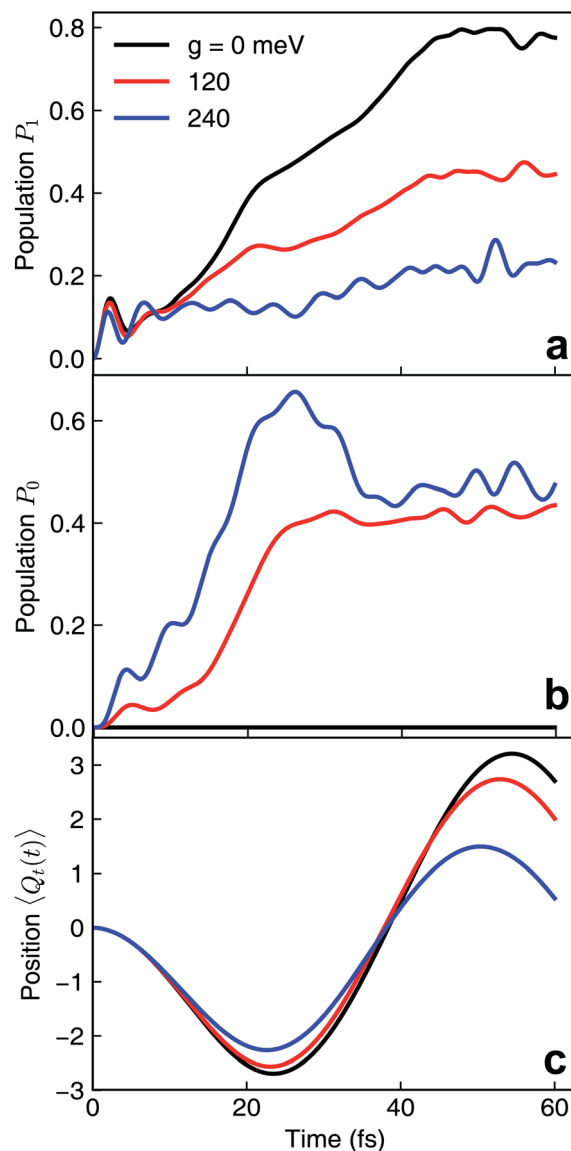


Fig. 2 Nonadiabatic polaritonic dynamics for the pyrazine model when a cavity mode with frequency $\omega_{\text{cav}} = 4.3$ eV couples to the $|\psi_0\rangle \leftrightarrow |\psi_1\rangle$ transition at different cavity–molecule coupling strength. (a and b) Population dynamics of electronic states (a) $|\psi_1\rangle$ and (b) $|\psi_0\rangle$. (c) Expectation value of the position of the tuning mode $\langle \Psi(t) | Q_t | \Psi(t) \rangle$ where $|\Psi(t)\rangle$ is the full polaritonic wavefunction.

relaxation dynamics accelerated by the strong coupling. The significant cavity-induced changes in the nonadiabatic dynamics can be understood from the shape of the PPESs. As shown in Fig. 3, the cavity–molecule coupling creates two new CIs in the PPESs. Distinct from the bare CI in the APES, these CIs are between a purely electronic state $|\psi_2\rangle$ and another polaritonic state with significant hybridization of matter and photon, as reflected in the color scheme which encodes the photon component in polaritonic states. More precisely, it corresponds to the expected photon number $N_{\text{ph}} = \langle \Phi(\mathbf{R}) | a_{\text{cav}}^\dagger a_{\text{cav}} | \Phi(\mathbf{R}) \rangle$ with the polaritonic state $|\Phi(\mathbf{R})\rangle$, which is a superposition of states $|\psi_0\rangle |1_{\text{cav}}\rangle$ and $|\psi_1\rangle |0_{\text{cav}}\rangle$. The polaritonic CIs play similar roles in the nonadiabatic polaritonic dynamics as CIs play in the nonadiabatic

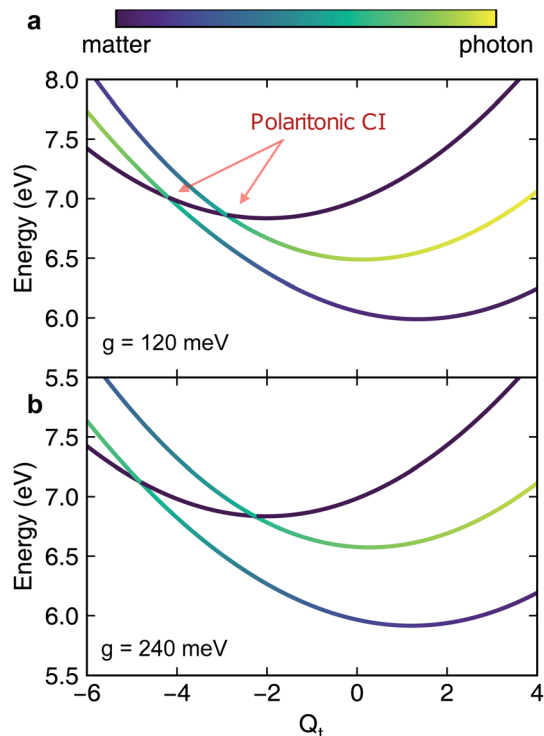


Fig. 3 Slices of the polaritonic potential energy surfaces along the tuning mode when the cavity mode couples to $|\psi_0\rangle \leftrightarrow |\psi_1\rangle$ at different light–matter coupling strength (a) $g \equiv g_{01} = 120$ meV and (b) $g = 240$ meV. Other parameters are $Q_c = 0$, $\omega_{\text{cav}} = 4.3$ eV. The pristine conical intersection (CI) in the adiabatic potential energy surfaces splits into a pair of novel polaritonic CIs in the polaritonic surfaces upon coupling to the cavity photon mode.

dynamics of pristine molecules. While CIs in APESs induce transitions between electronic states, polaritonic CIs induce transitions in the polaritonic surfaces. The nuclear wavepacket first traverses through one of the polaritonic CIs that is closer to the Franck–Condon point $\mathbf{R} \equiv (Q_c, Q_t) = (0, 0)$, part of the nuclear wavepacket relaxes to the third PPES (the ground surface is not shown in Fig. 3). Because the polaritonic states of this PPES consist of the contribution from $|\psi_0\rangle|1_{\text{cav}}\rangle$, the electronic ground state gains population during the course of dynamics. This picture is further confirmed by the expectation value of the position operator of the tuning mode. As the cavity–molecule coupling strength increases, the polaritonic CI is pushed further away from the pristine CI, thus explaining the increase of the average position of the nuclear wavepacket at $t \sim 25$ fs.

As the polaritonic CI is closer to the Franck–Condon point, the geometric phase effect is clearly observed in Fig. 4, which compares the nuclear probability density at $t = 32$ fs in electronic state $|S_1\rangle$ between the bare dynamics and the polaritonic dynamics ($g = 240$ meV). The nuclear probability density is obtained by tracing over the electronic and photonic degrees of freedom in the total wavefunction projected on the electronic subspace

$\mathcal{P} = |\psi_1\rangle\langle\psi_1|$, *i.e.*, $\rho_n(\mathbf{R}) = \int d\mathbf{r} \int d\mathbf{q} \left| \langle \mathbf{r}, \mathbf{q}, \mathbf{R} | \mathcal{P} \Psi(t) \rangle \right|^2$. The geometric phase effect is clearly seen in the vanishing of the probability along the $Q_c = 0$ line in the polaritonic dynamics

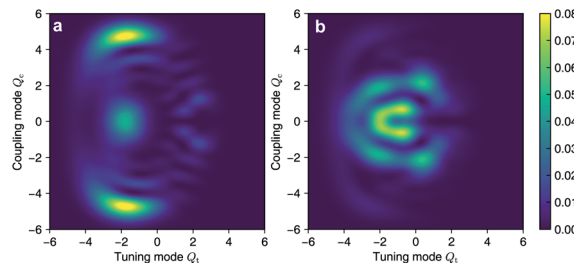


Fig. 4 Comparison of the nuclear probability density at $t = 32$ fs between (a) the bare dynamics and (b) the polaritonic dynamics at $g = 240$ meV. The geometric phase effect is clearly seen in the vanishing of probability along the $Q_c = 0$ line.

(Fig. 4b). The main difference is that $\rho_n(\mathbf{R})$ is less spread over the configuration space than the bare dynamics, meaning that less excitation energy flows into the vibrational modes. This is expected because part of the energy is contained in the cavity photon mode.

It is interesting to compare the novel polaritonic CI to the light-induced CI identified previously.^{1,31} In the latter case, the conical intersection is between two product states between the molecule and the cavity at configurations where the cavity–molecule interaction (transition dipole moments) vanishes. In other words, $|g\rangle \otimes |1_{\text{cav}}\rangle$ and $|e\rangle \otimes |0_{\text{cav}}\rangle$ are degenerate when $\boldsymbol{\mu}_{eg} \cdot \mathbf{e} = 0$, where $\boldsymbol{\mu}_{eg}$ is the transition dipole between states $|e\rangle$

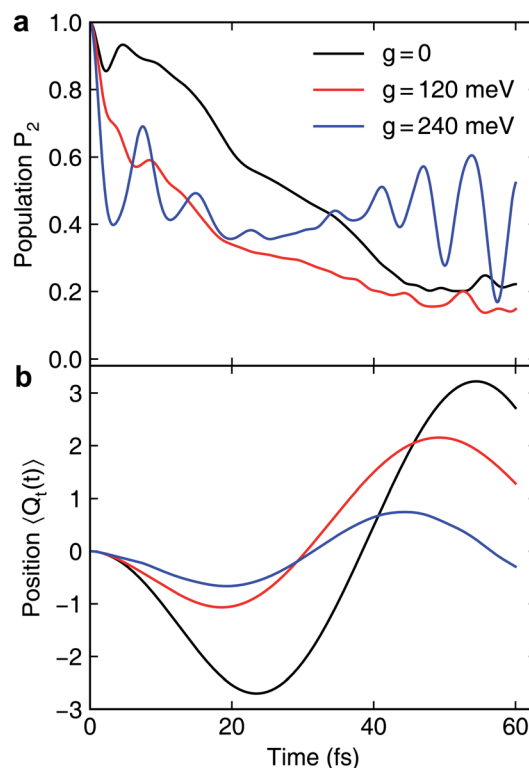


Fig. 5 Nonadiabatic polaritonic dynamics for the pyrazine model when the cavity mode couples to the $|\psi_1\rangle \leftrightarrow |\psi_2\rangle$ transition at different cavity–molecule coupling strength. (a) Population dynamics of electronic state $|\psi_2\rangle$. (b) Expectation value of the position of the tuning mode.

and $|g\rangle$ and \mathbf{e} is the polarization vector of the cavity photon mode, and the transition energy is resonant with the cavity photon energy. When one of the nuclear coordinates is a rotation, this CI can be realized at the angle where the transition dipole is orthogonal to the polarization of the cavity photon. It does not require a pristine CI in the molecule and the CI geometry is not affected by the light-matter coupling strength. In contrast, the novel pair of polaritonic CIs are between two hybrid polaritonic states. This emerges when the molecule itself contains a CI in the APESs and when the cavity mode couples to the transition between one of the APESs forming the bare CI and a third electronic state. Moreover, the polaritonic CIs geometry can be tuned by the strength of light-matter coupling strength. As the cavity-molecule coupling is increased to $g_{\text{cav}} = 240$ meV, the positions of the two polaritonic CIs are further apart. This change of the location of polaritonic CI can also be seen in the average position of the tuning mode, see Fig. 2c. Population relaxation to the ground electronic state is further increased.

We now turn to a different scenario where the cavity mode couples to the transition $|\psi_1\rangle \leftrightarrow |\psi_2\rangle$ transition. The PPESs are shown in Fig. 1d for $\omega_{\text{cav}} = 0.62$ eV (slightly lower than the transition frequency at the Frank-Condon point) and $g_{12} = 120$ meV. In this case, the ground electronic state is not playing any role in the dynamics as it is decoupled from the other electronic states. Upon turning on the light-matter interaction, we first observe a much faster electronic relaxation as shown in Fig. 5a. The relaxation time reduces from 30 fs without the cavity to ~ 15 fs at $g_{12} = 120$ meV. Interestingly, as can be seen from the average

position of the tuning mode in Fig. 5b, the nuclear wavepacket does not even reach the pristine conical intersection. Similar to the previous analysis, we interpret the nonadiabatic polaritonic dynamics from the shape of PPESs shown in Fig. 6. The main feature of the polaritonic surfaces is the emergence of a light-induced (avoided) crossing. This offers an additional electronic relaxation channel other than the pristine CI. Because the light-induced crossing is much closer to the Franck-Condon point in this case, the relaxation happens mainly through this channel and consequently, the relaxation happens much faster. As the coupling strength is enhanced, the relaxation rate is further increased.

Interestingly, this light-induced avoided crossing is always associated with a light-induced CI. This is because one can always rotate the molecule such that the transition dipole at the configuration \mathbf{R}^* , where the electronic transition is in resonance with the cavity photon energy, is orthogonal to the electric field polarization. Since we can always find such molecular geometry \mathbf{R}^* in an avoided crossing, the light-induced CI is guaranteed to exist.

For case II, the counterrotating terms that are neglected in the rotating-wave approximation [eqn (5)] may become important as the coupling strength becomes comparable to the cavity resonance (so-called ultrastrong coupling). To investigate the

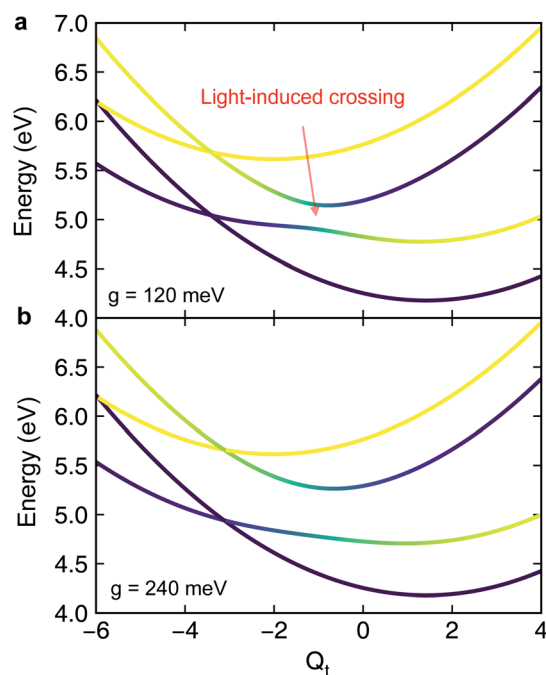


Fig. 6 Same as Fig. 3 but with the cavity photon mode coupling to the transition $|\psi_1\rangle \leftrightarrow |\psi_2\rangle$ and $g \equiv g_{12}$. The characteristic feature of the polaritonic surfaces is the light-induced crossing providing an additional channel for electronic relaxation.

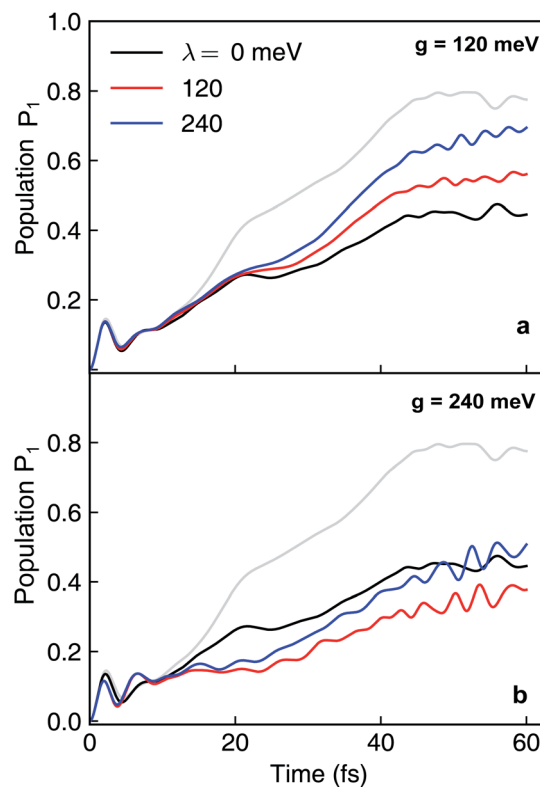


Fig. 7 Dissipative nonadiabatic polaritonic dynamics simulated by the hierarchical equations of motion when both the cavity mode and the external environment couples to the transition $|\psi_0\rangle \leftrightarrow |\psi_1\rangle$ at system-bath coupling strength $\lambda = 0, 120, 240$ meV. The grey line corresponds to the nonadiabatic dynamics of bare molecules without cavity. The cavity parameters are $\omega_{\text{cav}} = 4.3$ eV, the cavity-molecule couplings are (a) $g = 120$ meV and (b) $g = 240$ meV.

influences of counterrotating terms, we simulate the polaritonic dynamics employing the full interaction as in eqn (4). As shown in Fig. S2† where the dynamics with and without the RWA are contrasted, when $g = 120$ meV [Fig. S2(a and b)†], there is only minor changes in the polaritonic dynamics without invoking the RWA. For $g = 240$ meV [Fig. S2(c and d)†], the counterrotating terms start to play a role in the long-time dynamics $t > 40$ fs, but the initial relaxation dynamics ($t \in [0, 40]$ fs) remains almost the same.

3.2 Environmental effects

We now explore the external environmental effects on the nonadiabatic polaritonic dynamics. In our simulations, the environment is coupled to the same pair of electronic states that are coupled to the cavity photon mode. We note some common features that apply to all cases. First, even when the reorganization energy is twice the cavity–molecule coupling strength, *i.e.*, $\lambda/g = 2$, an appreciable difference between the bare dynamics and the polaritonic dynamics can still be observed implying that the cavity-controlled photochemistry can be robust to electronic decoherence. Further, while the environment is expected to destroy the phase coherence in a superposition of electronic states, it does not happen instantaneously and there is a characteristic timescale where the system dynamics is almost not influenced by the presence of environment, reminiscent of the quantum Zeno effects. This timescale can be estimated by the decoherence time for the environment to reduce an equal superposition

of a two-level system to a mixed state^{44,45} $\tau_c \sim 1/\sqrt{\lambda T}$. For $\lambda = 240$ meV, $T = 300$ K, $\tau_c \approx 9$ fs. This is consistent with the time where environmental effects becomes noticeable in the polaritonic dynamics.

Because the formation of cavity polaritons relies on the coherence between electronic states, the environment is expected to diminish the cavity control. This is indeed seen in the population dynamics of electronic state $|\psi_2\rangle$ in case I when $g = 120$ meV (Fig. 7a). When the cavity–molecule coupling is stronger, this deleterious effect becomes less significant (Fig. 7b). Another effect of the environment is reflected in case II where the coherent population transfer between electronics states $|\psi_2\rangle$ and $|\psi_1\rangle$ at $g = 240$ meV during the time periods 0–20 fs and 40–60 fs is reduced (Fig. 8b). The polaritonic dynamics at $g = 120$ meV in case II is almost immune to the external environment (Fig. 8a), the dissipative polaritonic dynamics for all system–bath coupling strengths $\lambda/g = 0, 1, 2$ shows the same timescale ~ 20 fs for the electronic relaxation in comparison to 40 fs in the bare molecule case. This implies that the relaxation channel provided by the light-induced crossing is robust to the environment.

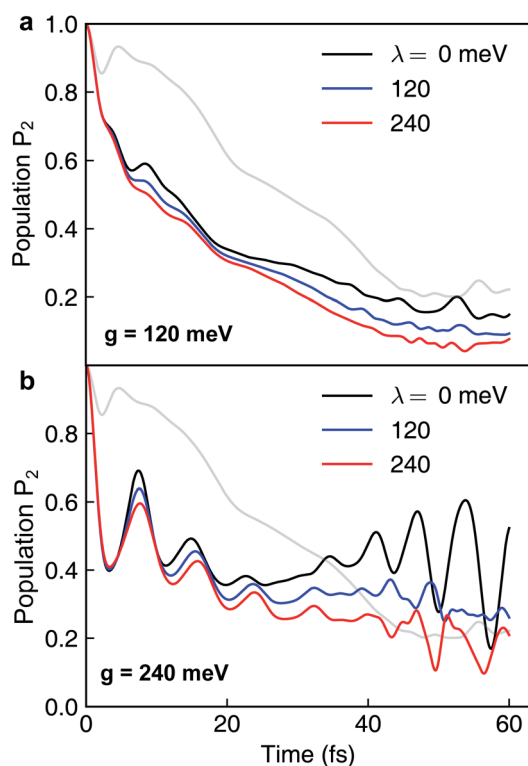


Fig. 8 Same as Fig. 7 but for both the cavity mode and the external environment coupled to the transition $|\psi_1\rangle \leftrightarrow |\psi_2\rangle$. The cavity parameters are $\omega_{\text{cav}} = 0.62$ eV, the cavity–molecule couplings are (a) $g = 120$ meV and (b) $g = 240$ meV.

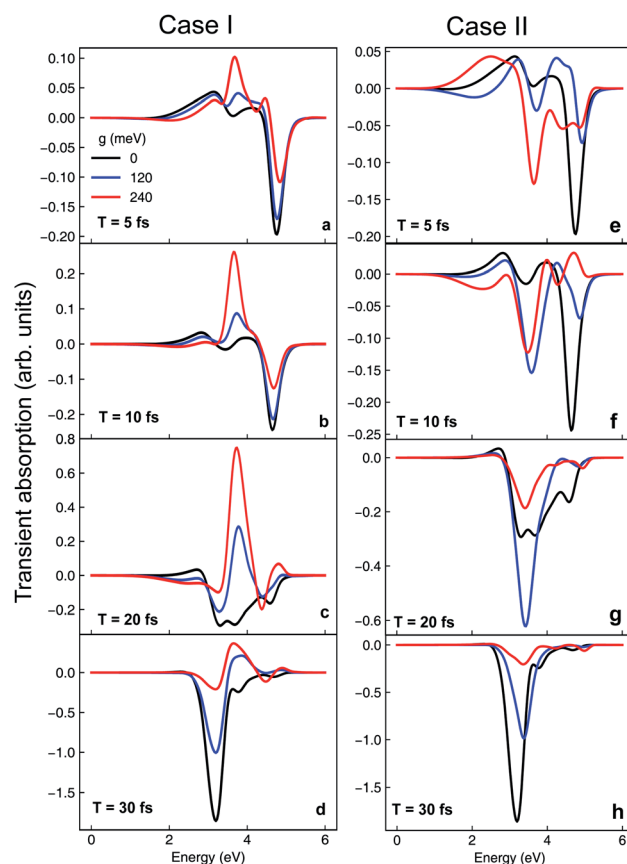


Fig. 9 Transient absorption spectra of the model pyrazine under strong coupling for case I (a–d) and II (e–h) at different cavity–molecule coupling strength. Here T is the time delay between the pump and probe pulses.

3.3 The transient absorption spectrum

The cavity-induced changes in the nonadiabatic dynamics can be clearly observed in TAS. Computational details of the TAS can be found in the ESI.† For pyrazine, the transition dipole between states $|\psi_0\rangle$ and $|\psi_2\rangle$ is much larger than the transition between $|\psi_0\rangle$ and $|\psi_1\rangle$. As shown in Fig. 9a–d, the main feature of the TAS for the bare nonadiabatic dynamics (*i.e.*, without the cavity) is a negative peak (stimulated emission) at ~ 3.2 eV growing during the course of dynamics accompanied by the diminishing of the stimulated emission peak at 4.8 eV. This arises from the stimulated emission from electronic state $|\psi_1\rangle$ to the ground state, and the increasing intensity corresponds to the population relaxation dynamics. In contrast, when the molecule is strongly coupled to the cavity as in case I, we observe a positive peak centered around 3.8 eV in the TAS. As a positive signal represents absorption of energy from the probe laser pulse, this feature is a signature of population relaxation to the ground electronic state. Further, when $g_{01} = 240$ meV (Fig. 9f), the absorption signal at $t = 20$ fs is much stronger than $g_{01} = 120$ meV, indicating that the relaxation to the ground state is faster with stronger coupling, consistent with the dynamics. The TAS for case II is shown in Fig. 9e–h. The stimulated emission $|\psi_1\rangle \rightarrow |\psi_0\rangle$ peak emerges as early as $T = 5$ fs (Fig. 9e), much earlier than the bare nonadiabatic dynamics, indicating that the relaxation is much faster when the molecule is under strong coupling, consistent with the picture of cavity-induced crossings.

4 Conclusions

To summarize, we have investigated how optical cavities can be used to manipulate the nonadiabatic molecular dynamics through a conical intersection. In contrast to a recent study⁴⁶ where the cavity is tuned to be in resonance with the Frank–Condon transition thus altering the initial photoexcitation, we investigated schemes where the molecules have to undergo a structural change to be in resonance with the cavity mode. By considering three electronic state model of pyrazine, we unveil that optical cavities, when coupled to the transition between one of the states comprising the CI and a third state, can split the pristine conical intersection in the APESs into two novel polaritonic conical intersections in the PPESSs. By tuning the cavity–molecule coupling strength, it is possible to vary the configurations of the polaritonic conical intersection pairs. This may serve as a novel control scheme to preserve electronic coherence in molecules because electronic coherence depends sensitively on the location of the CI.^{45,47,48} In the other case where the cavity photon couples to the two electronic states forming the CI, we found light-induced avoided crossings in the polaritonic potential energy surfaces, which provide additional relaxation channel for electronic excitation, and thus can accelerate the nonradiative relaxation dynamics. This light-induced crossing has also been suggested to manipulate the photoisomerization of azobenzene in a recent trajectory–surface hopping study.³¹ While the trajectory–surface hopping method cannot take electronic coherence as well as geometric phase

into account properly, our simulations do not suffer from such limitations.

We further explored the environmental effects on the polaritonic dynamics and demonstrated that even when the reorganization energy is larger than the cavity–molecule coupling, the optical cavities can still be employed to manipulate the photodynamics of molecules. Moreover, we showed that the TAS can be a useful spectroscopic technique to monitor the polaritonic dynamics. These results provide novel schemes to control the non-adiabatic dynamics with strong light–matter coupling, enriching the toolbox to use optical cavities to alter molecular properties and dynamics. Considering the rapid developments in nanophotonics,^{49,50} we expect that polaritonic systems can be experimentally investigated in the foreseeable future. The strong coupling can be also achieved through the collective interaction between many molecules and a single cavity mode, extending the proposed control schemes to photochemistry with many molecules will be investigated in the future.

Conflicts of interest

There are no conflicts to declare.

Acknowledgements

This work was supported by the National Science Foundation Grant CHE-1663822.

Notes and references

- 1 M. Kowalewski, K. Bennett and S. Mukamel, *J. Chem. Phys.*, 2016, **144**, 054309.
- 2 K. Bennett, M. Kowalewski and S. Mukamel, *Faraday Discuss.*, 2016, **194**, 259–282.
- 3 T. W. Ebbesen, *Acc. Chem. Res.*, 2016, **49**, 2403–2412.
- 4 X. Zhong, T. Chervy, S. Wang, J. George, A. Thomas, J. A. Hutchison, E. Devaux, C. Genet and T. W. Ebbesen, *Angew. Chem.*, 2016, **128**, 6310–6314.
- 5 X. Zhong, T. Chervy, L. Zhang, A. Thomas, J. George, C. Genet, J. A. Hutchison and T. W. Ebbesen, *Angew. Chem., Int. Ed.*, 2017, **56**, 9034–9038.
- 6 J. George, A. Shalabney, J. A. Hutchison, C. Genet and T. W. Ebbesen, *J. Phys. Chem. Lett.*, 2015, **6**, 1027–1031.
- 7 A. Shalabney, J. George, J. Hutchison, G. Pupillo, C. Genet and T. W. Ebbesen, *Nat. Commun.*, 2015, **6**, 5981.
- 8 F. Benz, M. K. Schmidt, A. Dreismann, R. Chikkaraddy, Y. Zhang, A. Demetriadou, C. Carnegie, H. Ohadi, B. de Nijs, R. Esteban, J. Aizpurua and J. J. Baumberg, *Science*, 2016, **354**, 726–729.
- 9 A. Thomas, L. Lethuillier-Karl, K. Nagarajan, R. M. A. Vergauwe, J. George, T. Chervy, A. Shalabney, E. Devaux, C. Genet, J. Moran and T. W. Ebbesen, *Science*, 2019, **363**, 615–619.
- 10 A. Shalabney, J. George, H. Hiura, J. A. Hutchison, C. Genet, P. Hellwig and T. W. Ebbesen, *Angew. Chem., Int. Ed.*, 2015, **54**, 7971–7975.

- 11 C. Schäfer, M. Ruggenthaler, H. Appel and A. Rubio, *Proc. Natl. Acad. Sci. U. S. A.*, 2019, **116**, 4883–4892.
- 12 J. Galego, F. J. Garcia-Vidal and J. Feist, *Phys. Rev. X*, 2015, **5**, 041022.
- 13 J. Flick and P. Narang, *Phys. Rev. Lett.*, 2018, **121**, 113002.
- 14 K. E. Dorfman and S. Mukamel, *Proc. Natl. Acad. Sci. U. S. A.*, 2018, **115**, 1451–1456.
- 15 F. Herrera and F. C. Spano, *Phys. Rev. Lett.*, 2016, **116**, 238301.
- 16 D. M. Coles, N. Somaschi, P. Michetti, C. Clark, P. G. Lagoudakis, P. G. Savvidis and D. G. Lidzey, *Nat. Mater.*, 2014, **13**, 712–719.
- 17 A. Frisk Kockum, A. Miranowicz, S. De Liberato, S. Savasta and F. Nori, *Nat. Rev. Phys.*, 2019, **1**, 19–40.
- 18 P. Vasa and C. Lienau, *ACS Photonics*, 2018, **5**, 2–23.
- 19 M. Hertzog, M. Wang, J. Mony and K. Börjesson, *Chem. Soc. Rev.*, 2019, **48**, 937–961.
- 20 J. A. Hutchison, T. Schwartz, C. Genet, E. Devaux and T. W. Ebbesen, *Angew. Chem., Int. Ed.*, 2012, **51**, 1592–1596.
- 21 J. Flick, M. Ruggenthaler, H. Appel and A. Rubio, *Proc. Natl. Acad. Sci. U. S. A.*, 2017, **114**, 3026–3034.
- 22 T. Schwartz, J. A. Hutchison, J. Léonard, C. Genet, S. Haacke and T. W. Ebbesen, *ChemPhysChem*, 2013, **14**, 125–131.
- 23 F. Herrera and F. C. Spano, *ACS Photonics*, 2018, **5**, 65–79.
- 24 L. A. Martínez-Martínez, M. Du, R. F. Ribeiro, S. Kéna-Cohen and J. Yuen-Zhou, *J. Phys. Chem. Lett.*, 2018, **9**, 1951–1957.
- 25 D. Sanvitto and S. Kéna-Cohen, *Nat. Mater.*, 2016, **15**, 1061–1073.
- 26 A. Mandal and P. Huo, *J. Phys. Chem. Lett.*, 2019, **10**, 5519–5529.
- 27 M. Du, R. F. Ribeiro and J. Yuen-Zhou, *Chem*, 2019, **5**, 1167–1181.
- 28 J. B. Pérez-Sánchez and J. Yuen-Zhou, arXiv: 1909.13024, 2019.
- 29 O. Vendrell, *Phys. Rev. Lett.*, 2018, **121**, 253001.
- 30 T. Szidarovszky, G. J. Halász, A. G. Császár, L. S. Cederbaum and Á. Vibók, *J. Phys. Chem. Lett.*, 2018, **9**, 6215–6223.
- 31 J. Fregoni, G. Granucci, E. Cocchia, M. Persico and S. Corni, *Nat. Commun.*, 2018, **9**, 4688.
- 32 Y. Tanimura, *J. Phys. Soc. Jpn.*, 2006, **75**, 082001.
- 33 Y. Tanimura and R. Kubo, *J. Phys. Soc. Jpn.*, 1989, **58**, 101–114.
- 34 C. Woywod, W. Domcke, A. L. Sobolewski and H.-J. Werner, *J. Chem. Phys.*, 1994, **100**, 1400–1413.
- 35 L. Chen, M. F. Gelin, V. Y. Chernyak, W. Domcke and Y. Zhao, *Faraday Discuss.*, 2016, **194**, 61–80.
- 36 M. Sala and D. Egorova, *Chem. Phys.*, 2016, **481**, 206–217.
- 37 J. Flick, H. Appel, M. Ruggenthaler and A. Rubio, *J. Chem. Theory Comput.*, 2017, **13**, 1616–1625.
- 38 K. Bennett, M. Kowalewski and S. Mukamel, *J. Chem. Theory Comput.*, 2016, **12**, 740–752.
- 39 H.-P. Breuer and F. Petruccione, *The Theory of Open Quantum Systems*, Oxford University Press, 2002.
- 40 B. Gu and I. Franco, *J. Chem. Phys.*, 2019, **151**, 014109.
- 41 W. Hu, B. Gu and I. Franco, *J. Chem. Phys.*, 2018, **148**, 134304.
- 42 Y. Tanimura and S. Mukamel, *J. Chem. Phys.*, 1993, **99**, 9496–9511.
- 43 Z. Wang, W. Wu, G. Cui and J. Wang, *New J. Phys.*, 2018, **20**, 033034.
- 44 O. V. Prezhdo and P. J. Rossky, *Phys. Rev. Lett.*, 1998, **81**, 5294–5297.
- 45 B. Gu and I. Franco, *J. Phys. Chem. Lett.*, 2018, **9**, 773–778.
- 46 I. S. Ulusoy, J. A. Gomez and O. Vendrell, *J. Phys. Chem. A*, 2019, **123**, 8832–8844.
- 47 C. Arnold, O. Vendrell, R. Welsch and R. Santra, *Phys. Rev. Lett.*, 2018, **120**, 123001.
- 48 B. Gu and I. Franco, *J. Phys. Chem. Lett.*, 2017, **8**, 4289–4294.
- 49 P. Forn-Díaz, L. Lamata, E. Rico, J. Kono and E. Solano, *Rev. Mod. Phys.*, 2019, **91**, 025005.
- 50 R. Chikkaraddy, B. de Nijs, F. Benz, S. J. Barrow, O. A. Scherman, E. Rosta, A. Demetriadou, P. Fox, O. Hess and J. J. Baumberg, *Nature*, 2016, **535**, 127–130.